Analytical and Bioanalytical Chemistry
https://doi.org/10.1007/s00216-019-02146-w

RESEARCH PAPER

Electrochemical biosensor for amplified detection of Pb^{2+} based on perfect match of reduced graphene oxide–gold nanoparticles and single-stranded DNAzyme

Cui Lai[1,2] · Yujin Zhang[1,2] · Xigui Liu[1,2] · Shiyu Liu[1,2] · Bisheng Li[1,2] · Mingming Zhang[1,2] · Lei Qin[1,2] · Huan Yi[1,2] · Minfang Li[1,2] · Ling Li[1,2] · Yukui Fu[1,2] · Jiangfan He[1,2] · Liang Chen[3]

Received: 21 May 2019 / Revised: 8 August 2019 / Accepted: 9 September 2019

Abstract

In this study, a sensitive amplification strategy for Pb^{2+} detection using reduced graphene oxide (RGO) and gold nanoparticles (AuNPs) was proposed. Thiol-modified DNAzyme is specific for Pb^{2+} self-assembly on RGO-AuNPs-modified electrode surface. Ferrocene labeled single-stranded DNAzyme (Fc-ssDNAzyme) self-hybridizes to form a DNA hairpin structure. The amount of Fc adsorbed on the electrode surface changes after the appearance of Pb^{2+}, leading to a change of electrical signal. This change can be sensitively identified by differential pulse voltammetry (DPV) assisted by ferricyanide ($[Fe(CN)_6]^{3-/4-}$) in the electrolyte. The high conductivity and specific surface area of RGO and the strong chemical bond adsorption effect between DNAzyme and AuNPs are responsible for the amplified detection of Pb^{2+}, which realize a detection range of 0.05–400,000.0 nM and a minimum detection limit of 0.015 nM. Moreover, the selectivity test results indicated that the biosensor had specificity for Pb^{2+}, even if there was interference from other high-concentration metal ions. This simple biosensor also exhibited good responsiveness in actual sample detection, which provides a good application prospect for field detection of Pb^{2+} in water.

Keywords Pb^{2+} · Reduced graphene oxide · Gold nanoparticles · Ferrocene-labeled single-stranded DNAzyme · Redox charge of $[Fe(CN)_6]^{3-/4-}$

Introduction

Pb^{2+} pollution is an environmental problem over the world, and there are many risks endangering people's health [1]. Pb^{2+} poisoning is related to neurological, cardiovascular, mental, reproductive, and developmental disorders, causing serious harm to liver, kidney, and other organs [2]. Children, in particular, are more vulnerable to Pb^{2+} and may suffer from amnesia, anemia, muscle paralysis, and mental retardation [3, 4]. The maximum pollution level of Pb^{2+} in drinking water is defined by the US Environmental Protection Agency (EPA) as 72 nM [5, 6]. Therefore, it is necessary to exploit ultra-sensitive and excellent selective methods for the detection of Pb^{2+} in water.

At present, the most common techniques used for detecting Pb^{2+} are atomic absorption spectrometry (AAS), inductively coupled plasma optical emission spectrometry (ICP-OES), inductively coupled plasma mass spectrometry (ICP-MS), inductively coupled plasma atomic emission spectrometry (ICP-AES), and X-ray fluorescence spectrometry (XRF) [7, 8]. Although these methods are sensitive and precise for the determination of Pb^{2+}, they rely on expensive instruments and complex sample preparation processes [9, 10]. Therefore, many new and simpler methods for the detection of Pb^{2+} have emerged, such as colorimetric method [7, 11], fluorescence method [12, 13], electrochemical method [14–16], and photoelectrochemical method [17, 18]. Within them, electrochemical method has drew much

Electronic supplementary material The online version of this article (https://doi.org/10.1007/s00216-019-02146-w) contains supplementary material, which is available to authorized users.

✉ Cui Lai
laicui@hnu.edu.cn

[1] College of Environmental Science and Engineering, Hunan University, Changsha 410082, Hunan, China

[2] Key Laboratory of Environmental Biology and Pollution Control, Ministry of Education, Hunan University, Changsha 410082, Hunan, China

[3] Faculty of Life Science and Technology, Central South University of Forestry and Technology, Changsha 410004, Hunan, China

Published online: 21 October 2019

attention on account of its mature theory, simple pretreatment, simple design, convenient measurement, high sensibility, and good selectivity [19, 20].

DNAzyme has been widely used in electrochemical detection. DNAzyme (also known as catalytic DNA) is an artificial deoxyribonuclease, which is a simple single-strand DNA (ssDNA) sequence obtained by vitro screening [21]. DNAzyme can catalyze the cleavage of its zymolyte chain with the help of specific metal ions (as cofactors), showing eminent affinity and specificity to metal ions [22, 23]. It is well known that Pb^{2+} can assist 8–17 DNAzyme to catalyze its substrate lysis [24, 25]. Zhang and colleagues developed an electrochemical biosensor by using 8–17 DNAzyme-modified gold electrode as the amplification method for detecting Pb^{2+}, making the detection limit reached 0.25 nM [21]. Our team also designed a Pb^{2+} amplification detection biosensor based on nanoporous gold modified electrode to connect 8–17 DNAzyme modified by gold nanoparticles (AuNPs). The detection limit was relatively low at 0.012 nM [26]. Therefore, the prepared 8–17 DNAzyme-based biosensors have been widely used for Pb^{2+} detection with outstanding sensibility and selectivity. In the process of developing high sensitivity electrochemical biosensors, the amplification strategy for detection has always been the focus of research [27–29]. Using nanomaterials (such as metal nanomaterials, carbon nanomaterials, and various quantum dots) to construct electrode sensing platforms and carriers to realize signal amplification has been widely developed [9, 30, 31]. Reduced graphene oxide (RGO) is often utilized as an electronic medium to modify electrodes and has been widely used in electrochemical sensors [32, 33]. RGO has the advantages of high conductivity, high ratio superficial area, low preparation cost, strong adsorption ability, good mechanical strength, good electrochemical stability, etc. [34–36]. Compared with RGO, graphene is a single-carbon layer with graphite structure, which is obtained by mechanical cracking and has low yield. Graphene oxide has poor conductivity due to the existence of many functional groups on its surface. Therefore, RGO has certain advantages in electrochemical analysis and determination [37, 38]. Many researches had used RGO and specific DNA strand for electrochemical amplification detection of targets. Gao and co-workers used thionine as the signal molecule and RGO as the signal enhancement platform. Besides, the G-rich ssDNA conformation induced by Pb^{2+} was utilized to construct the Pb^{2+} electrochemical biosensor, realizing the minimum detection limit of 0.032 pM [39]. Zhang et al. proposed a simple signal-off electrochemical biosensor for Hg^{2+} detection based on the thymine-mercuric-thymine hybridization directly on RGO. The detection limit was 5 pM [40]. Interestingly, the interaction between RGO and ssDNA is stronger than that of double-stranded DNA (dsDNA). ssDNA is stably adsorbed by RGO and this is attributed to the π-stack among the ring construction of the basic groups and the hexagon cells of RGO. In contrast, dsDNA does not bind to RGO stably and retains its spiral structure because the basic groups are blocked in the phosphate backbone of dsDNA [41]. However, in this work, the modified 8–17 DNAzyme which added 6 nucleobases at the 3′ end of the enzyme chain and connected to the 5′ end of the substrate chain cannot be effectively adsorbed by RGO, because the substrate chain and the enzyme chain can be spontaneously assembled into a hairpin structure. Although the use of modified 8–17 DNAzyme could reduce the impact of DNAzyme inactivation and cumbersome DNAzyme processing steps, it cannot be stably adsorbed on RGO surface due to its double-strand-like structure. To enable that both single and double strands of DNA can be connected to RGO, functional groups need to be added to RGO. For example, Wang and colleagues developed an electrochemical biosensor for double determine Pb^{2+} and Hg^{2+} with amino-modified RGO (through nitrogen plasma enhanced chemical vapor deposition method), DNAzyme, and ion-specific DNA-modified gold electrode, with the detection limit of 7.8 pM and 5.4 pM, respectively [2]. However, in the process of adding the amino group, there are not only the usual thermochemical reactions on the surface of RGO but also complex plasma chemical reactions. Rasheed and colleagues developed an electrochemical biosensor that can detect 1 femtomolar BRCA1 gene (about 5.896 fg mL^{-1}) by using amino RGO and BRCA1 DNA [42]. Benvidi and colleagues connected DNA chain of Amelogenin gene and RGO by activating carboxylic acid groups on the RGO surface, so as to achieve the detection limit of 0.0032 aM for the electrochemical biosensor of the Amelogenin gene. But when the carboxyl groups are activated, some RGO particles will be lost due to immersing and washing process [43].

In this study, we proposed a simpler electrochemical method for Pb^{2+} detection. A layer of AuNPs was electrodeposited on the RGO surface (RGO-AuNPs) [44], and Au-S coordination bond was used to better connect the thiolated DNAzyme [45]. Compared with silver nanoparticles, platinum nanoparticles, copper nanoparticles, and other nanomaterials, AuNPs have the advantages of easy functionalization, high stability, short synthesis cycle, appropriate price, and good electrical conductivity [46–49]. Moreover, the 3′ end of ssDNAzyme was modified with the signal molecule ferrocene (Fc-ssDNAzyme) to enhance the sensibility of the biosensor [40]. In the presence of Pb^{2+}, the rA in Fc-ssDNAzyme is recognized and cut off, resulting in the departure of Fc with a segment of DNA and the change in the electrical signals on the electrode surface. Furthermore, the biosensor was also improved in electrochemical differential pulse voltammetry (DPV) test by adding ferricyanide ($[Fe(CN)_6]^{3-/4-}$) into the electrolyte because the subtle change on the electrode surface can be detected more sensitively [50]. In summary, Pb^{2+} electrochemical biosensor was prepared by modifying electrode with RGO-AuNPs and Fc-ssDNAzyme, and the DPV test method was used to measure the current value in the electrolyte containing

ferricyanide. The modified electrode has good sensitivity and selectivity due to its high conductivity and large loading of surface specific active substances. In addition, the sensitivity is further improved due to the presence of signal molecules and redox probes. Compared with previous studies [2, 21, 51], the designed Pb^{2+} biosensor has wide detection range, low detection limit, and simple operation.

Experimental section

Materials and apparatus

The oligonucleotide used in the experiment was synthesized by the Sangon Biotech. Co., Ltd. (Shanghai, China) and purified by high-performance liquid chromatography (HPLC). The Pb^{2+}-specific ssDNAzyme (probe: P) sequence: 5′-SH-$(CH_2)_6$-CATCTCTTC-TCCGAGCCGGTCGAA-ATAGTGAGT-TTTTTT-ACTCACTAT-rA-GGAAGAGA TG-Fc-3′. The probe contains a substrate chain (the part of oligonucleotide chain that contains the rA) and a catalytic enzyme chain. rA is ribonucleotide adenine. Fc is ferrocene. Tris (2-carboxyethyl) phosphine hydrochloride (TCEP) and 6-hercapto-1-hexanol (MCH) were obtained from Sigma-Aldrich Chemical Co. Pb^{2+} standard solution was obtained from Central Iron & Steel Research Institute (Beijing, China). Graphite powder, $AgNO_3$, $AlCl_3$, $CaCl_2$, $CdCl_2$, $CoCl_2$, $CuCl_2$, $FeCl_3$, $Hg(NO_3)_2$, KCl, $MgSO_4$, $MnCl_2$, $NiCl_2$, and $ZnSO_4$ were obtained from Sinopharm Chemical Reagent Co., Ltd. (Shanghai, China). Chloroauric acid hydrated ($HAuCl_4{\cdot}4H_2O$) was purchased from Sinopharm Chemical Reagent Co., Ltd. (Beijing, China). The other chemicals involved were analytical grade and had not been further purified. Ultra-pure water (18.25 MΩ cm) was used in the entire experiment. The buffers used in the experiment were as follows: Tris-EDTA buffer solution (TE, 10 mM Tris-HCl, 1 mM EDTA, pH 8.0), annealing buffer solution (10 mM Tris, 50 mM NaCl, 1 mM EDTA, pH 7.5–8.0), 10 mM Tris-acetate buffer solution (pH 8.0), 50 mM Tris-acetate buffer solution (pH 7.5, containing 50 mM NaCl), and phosphate buffer saline solution (PBS, 100 mM, pH 7.4).

The electrochemical test was implemented on the CHI760E electrochemical workstation of China Chenhua Instruments Co., Ltd. The three electrodes used were glass carbon electrode (GCE, diameter 3 mm) as working electrode, saturated calomel electrode (SCE) as reference electrode, and platinum wire counter electrode, respectively. The morphology of RGO and AuNPs/RGO were observed by JEOL JEM-3010 transmission electron microscopy (TEM) (JEOL Ltd., Japan) and scanning electron microscope (SEM) (Hitachi S-4800). If not specified, the tests were implemented at room temperature (25 °C).

Preparation of RGO

Graphene oxide (GO) was synthesized from graphite powder by improved Hummers method [52, 53]. Firstly, 2.5 g of graphite was added to the concentrated H_2SO_4 (60 mL) while stirring slowly and cooling in ice water, then slowly added 1.25 g of KNO_3 and 7.5 g of $KMnO_4$ (for more than 30 min). After stirring at 35 °C for 1 h, 120 mL of H_2O was added to the suspension, and the temperature was raised to 95 °C and held for 30 min. The suspension was then diluted with 350 mL of H_2O and treated with 100 mL 6% of H_2O_2 to reduce the residual potassium permanganate and manganese dioxide. The suspension was filtrated and washed with 1 M HCl and H_2O. Later, GO powder was obtained after vacuum drying the filter residue.

RGO was synthesized by a chemical reduction of GO with hydrazine as reductant [54]. In short, 150 mg of GO and 100 mL of ultra-pure water were added to the flask and dispersed by ultrasound for 2 h. Then added 3 mL of hydrazine solution to the flask and mixed evenly. The solution turned black. The solution was then stirred in an oil bath of 95 °C, refluxed for 24 h, and filtered. The filter residue was washed several times with 500 mL of H_2O and 500 mL of methanol, respectively, and dried at 60 °C. The synthetic RGO was distributed in ultra-pure water for 20 h through ultrasound.

Biosensor fabrication

The GCE surface was polished with 0.05 μm alumina slurry until the mirror surface appeared and then washed with ultra-pure water. Ultrasound was then performed in ethanol and ultra-pure water for approximately 5 min, respectively, to remove any attached particles. The clean bare electrode was prepared by nitrogen drying, which is ready for further modification. Ultrasonic treatment of RGO (1 mg mL^{-1}) for about 30 min, resulting in uniform dispersion. Then 12 μL of RGO was dripped onto the GCE surface by physical adsorption and evaporated completely for about 1 h at room temperature. A uniform thin layer of RGO was prepared on the GCE surface (RGO/GCE) [55]. Subsequently, AuNPs were electrodeposited on RGO-modified GCE by cyclic voltammetry (CV) in a solution containing 1% (w/v) $HAuCl_4$ (AuNPs/RGO/GCE) (potential 0 to 1.6 V, scanning rate 0.02 V s^{-1}, potential cycle 3), and the $HAuCl_4$ solution could be reused [56]. Besides, DNAzyme solution (100 μM, diluted via TE buffer solution) was mixed in annealing buffer solution, kept at 95 °C for 5 min, then gradually cooled to room temperature to obtain 10 μM DNAzyme (formed as many hybrid hairpin structures as possible), which was cryopreserved [15, 57]. When used, the working fluid was 1 μM DNAzyme obtained through further dilution, containing 10 mM Tris-acetate buffer (pH 8.0) and 1 mM TCEP (reduced disulfide bond oligomer) [58], and placed under shading for 2 h [59]. Then AuNPs/

RGO/GCE electrode was self-assembled with 10 μL thiol-modified Fc-ssDNAzyme at 4 °C for 12 h to obtain P/AuNPs/RGO/GCE electrode. Afterwards, the electrode was passivated with 2 mM MCH for 1 h (which is to prevent nonspecific contact between the DNA skeleton and the electrode surface) [60]. Finally, the nonspecific adsorption of DNAzyme was removed by washing with 10 mM Tris-acetate buffer (pH 8.0).

Procedures for Pb^{2+} detection

Firstly, the modified electrode reacted with 200 μL different concentrations of Pb^{2+} (adding quantitative Pb^{2+} standard solution in ultra-pure water) at 37 °C for 40 min. The electrode was then cultured in buffer solution (10 mM Tris-acetate, pH 8. 0) for 5 min to remove the loose single-stranded DNAzyme after cleavage. In the sensitivity test, the concentrations of Pb^{2+} included 0, 0.05, 0.1, 0.5, 1.0, 5.0, 10.0, 50.0, 100.0, 500.0, 1000.0, 5000.0, 10,000.0, 50,000.0, 100,000.0, and 400,000.0 nM. The prepared electrodes were then tested with DPV in 100 mM PBS buffer (pH 7.4) containing 5 mM $[Fe(CN)_6]^{3-/4-}$ (1:1) and 10 mM KCl. Some of the parameters of DPV were set as follows: the measurement range was from − 200 to 600 mV, the amplitude was 50 mV, and the pulse width was 50 ms. Besides, CV was used to characterize the electrode, the potential measuring range was from − 0.3 to 0.8 V, and the scanning rate was 50 mV s^{-1}. Electrochemical impedance spectroscopy (EIS) was utilized to characterize the step-by-step modification performance of the electrode. The frequency range was from 0.1 Hz to 100 kHz with 5 mV of amplitude, the initial potential was 0.20 V. CV and EIS were also measured in 100 mM PBS buffer (pH 7.4) containing 5 mM $[Fe(CN)_6]^{3-/4-}$ (1:1) and 10 mM KCl. DPV was used to optimize the experimental conditions and determine the selectivity, reproducibility, and stability of the proposed biosensor.

Environmental sample analysis

The three kinds of actual water samples used in the experiment were river water, lake water, and tap water. The river water came from the Xiangjiang River in Changsha, China. The lake water came from Peach Lake in Changsha, China. And the tap water came from our laboratory in Changsha, China. After taking it back, the water samples were filtered immediately to remove some solid suspended matter, and then different concentrations of Pb^{2+} were added. The proposed biosensor was utilized for detecting the content of Pb^{2+} in these water samples.

Results and discussion

Experimental principle and sensing scheme

In this experiment, an electrochemical biosensor for Pb^{2+} detection was prepared with Pb^{2+}-specific ssDNAzyme (3′-Fc, 5′-SH). The schematic diagram of the biosensor was shown in Scheme 1. RGO was physically adsorbed onto the polished GCE. RGO solution which had been ultrasonically treated for 20 h was used in this experiment, where RGO had been evenly dispersed and a relatively stable film can be formed on the surface of GCE. We had tried to add adhesive to RGO solution, such as Nafion, but the decline in conductivity of the complex suggested that this was not a satisfactory attempt. AuNPs were electrodeposited on the RGO-modified GCE, and then DNAzyme was self-assembled on the electrode by Au-S bond. After treatment with MCH, DNAzyme was assembled vertically on the AuNPs/RGO electrode [61]. When the prepared P/AuNPs/RGO electrode was cultured with Pb^{2+} solution, the substrate chain was broken down at scissile rA point. For the biosensor, RGO improved conductivity and specific surface area of GCE. AuNPs enabled a large number of Fc-ssDNAzymes were connected to the surface of AuNPs/RGO electrode. Fc provided the signal molecules. In the presence of Pb^{2+}, the Fc is removed from the electrode surface, and the redox charge $[Fe(CN)_6]^{3-/4-}$ can move on the surface of electrode with a lower electron transfer resistance. As a result, the electrical signal increases [39]. Therefore, the biosensor realized the ultra-sensitive amplification detection of Pb^{2+}.

Characterization of the RGO-AuNPs based biosensor

RGO is a good electron-mediated material because of its strong conductivity. In addition, it has a high ratio superficial area. The surface morphology of RGO was tested by TEM (see Electronic Supplementary Material (ESM) Fig. S1A). As shown in Fig. S1A, lamellar structures similar to thousand lake islands and water ripples can be seen. The morphology of RGO folded like this was conducive to the combination of more AuNPs [40]. Figure S1B and Fig. S1C (see ESM) were the SEM images of RGO and AuNPs/RGO, respectively, indicating that AuNPs had been successfully and uniformly electrodeposited on the RGO-modified electrode.

The performance of RGO and AuNPs-modified electrode was tested by CV. Figure 1 revealed the test results of the redox probe $[Fe(CN)_6]^{3-/4-}$ at bare GCE, RGO/GCE, AuNPs/GCE, and AuNPs/RGO/GCE, respectively. As can be seen from Fig. 1, the current peak value of RGO/GCE was 1.67 times of bare GCE, which is due to the strong conductivity of RGO. However, the current peak value of AuNPs/RGO/GCE (1.31 times of bare GCE) was less than that of RGO/GCE. The RGO layer was first dropped onto the

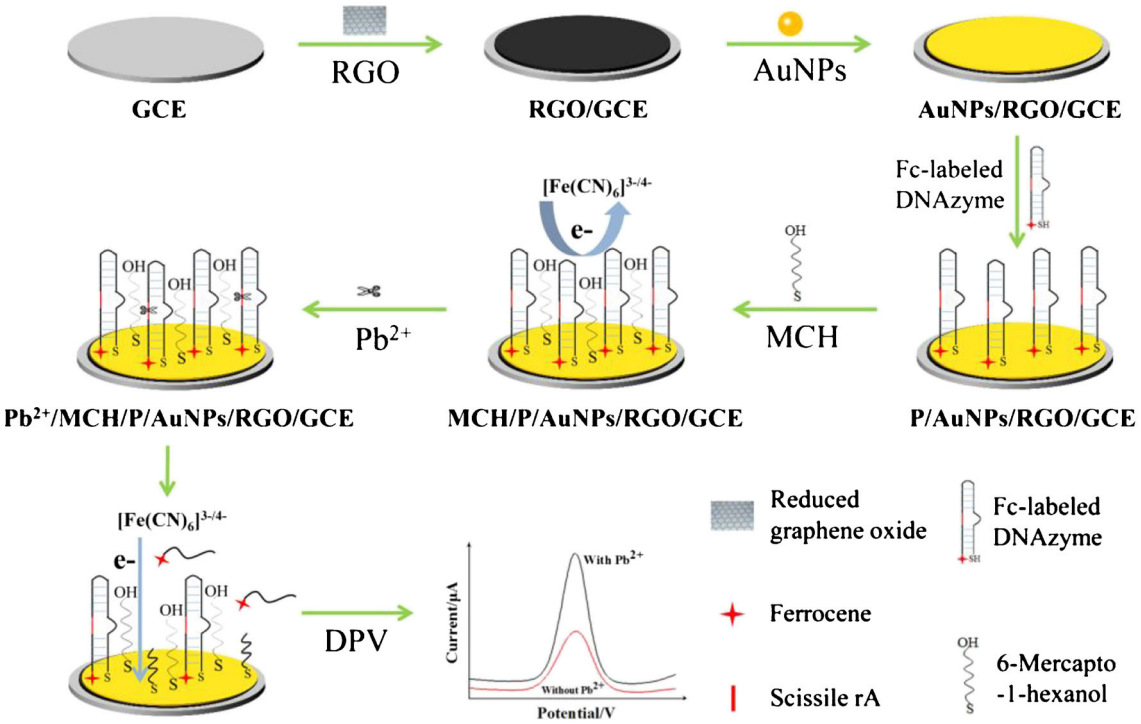

Scheme 1 Schematic diagram of preparation process of Pb^{2+} detection biosensor

electrode surface, and then a layer of dense AuNPs was electrodeposited. The coverage of AuNPs will hinder the high conductivity of RGO. Accordingly, the current value of AuNPs/RGO/GCE was smaller than that of RGO/GCE [62]. In short, the current peak value of AuNPs/RGO/GCE (curve d) was greater than that of bare GCE (curve a), indicating that the AuNPs/RGO was successfully modified onto the GCE surface.

The layer-by-layer assembly process of biosensor was tested by EIS. Figure 2 exhibited the Nyquist diagram of the layer-by-layer modified electrode in PBS solution containing 5 mM $[Fe(CN)_6]^{3-/4-}$ (1:1) and 10 mM KCl at frequencies from 0.01 Hz to 100 kHz. The impedance spectrum can be simulated by equivalent circuit [63]. Concretely, the equivalent circuit consists of four parts: charge transfer resistance (R_{CT}), Warburg impedance (Z_w), electrolyte ohmic resistance (R_s), and interface capacitance (C_{dl}). There are two parts in the impedance spectrum: semicircle and straight line. R_{CT} represents the diameter of the semicircle in the diagram. A straight line

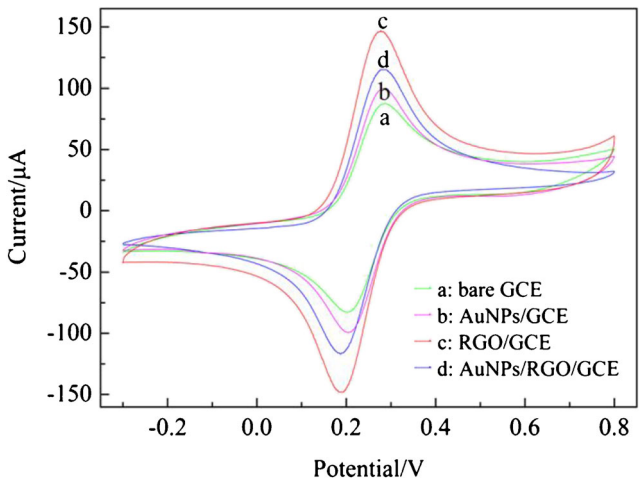

Fig. 1 Cyclic voltammograms of bare GCE (**a**), AuNPs/GCE (**b**), RGO/GCE (**c**), and AuNPs/RGO/GCE (**d**)-modified electrode in 100 mM PBS buffer solution (pH 7.4) containing 5 mM $[Fe(CN)_6]^{3-/4-}$ (1:1) and 10 mM KCl at a scan rate of 50 mV s^{-1}

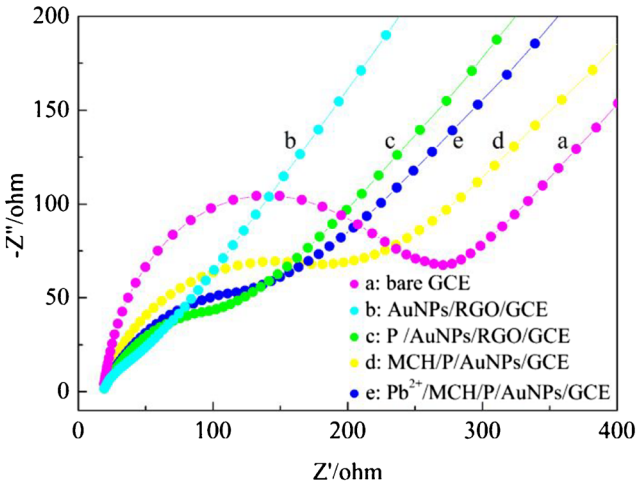

Fig. 2 Electrochemical impedance spectra (Nyquist plots) of bare GCE (**a**), AuNPs/RGO/GCE (**b**), P/AuNPs/RGO/GCE (**c**), MCH/P/AuNPs/RGO/GCE (**d**), and MCH/P/AuNPs/RGO/GCE after incubating with Pb^{2+} (**e**) with frequency range from 0.01 Hz to 100 KHz

represents a diffusion process. By fitting the impedance spectrum with the equivalent circuit diagram (ESM Fig. S2A), the corresponding values of each element in the equivalent circuit diagram can be obtained (ESM Table S1). The R_{CT} of bare GCE was about 227 Ω (curve a), which indicated the R_{CT} was very large. After GCE was modified with AuNPs/RGO, the semicircle decreased a lot (curve b), showing that the electron transfer rate was increased, and the AuNPs/RGO combination improved the conductivity of GCE. After self-assembly of Fc-ssDNAzyme, the diameter of semicircle increased (curve c), which was due to the electrostatic repulsion among negatively charged oligonucleotides and redox couple $[Fe(CN)_6]^{3-/4-}$, hindering the charge transfer. When the modified electrode was cultured with non-conductive MCH, the surface of the electrode was almost insulated, so the R_{CT} increased further (curve d). However, after the addition of Pb^{2+}, the R_{CT} was decreased (curve e). This was because Pb^{2+} damaged the hybrid hairpin structure, leading to irreversible breakage. In this way, a large number of unstructured nucleotides were formed and removed from the electrode surface. Meanwhile, the electrostatic repulsive force was reduced, and the R_{CT} was reduced accordingly. These experimental results demonstrated that the surface modification of GCE had been successfully carried out [38, 64].

The experiment of electrode surface coverage measurement was also carried out. Figure 3 illustrated the relationship between the current peak values and the scanning rates (v) (10 to 250 mV s^{-1}), where I_{pc} (μA) = 427.4958 v (mV s^{-1}) + 35.28369, R^2 = 0.99184; I_{pa} (μA) = − 314.57777 v (mV s^{-1}) − 40.59521, R^2 = 0.98524. The relevant theoretical equation was as follows:

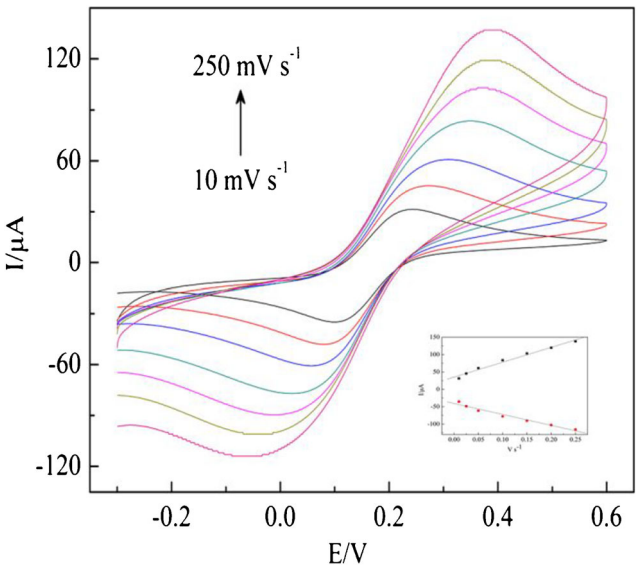

Fig. 3 Cyclic voltammograms of RGO-AuNPs and Fc-ssDNAzyme-modified GCE at various scan rates (10, 25, 50, 100, 150, 200, and 250 mV s^{-1}) in 50 mM Tris-acetate (pH 7.5, 50 mM NaCl, 5 mM $[Fe(CN)_6]^{3-/4-}$ (1:1), and 10 mM KCl). Inset: the curves of redox peak currents vs scan rates

$$I_p = n^2 F^2 v A \Gamma / 4RT \quad (1)$$

Concretely, n is the number of charge transfer, F is the Faraday constant, v is the scanning rate, A is the surface area of the electrode, Γ is the surface active coverage, R is the gas constant, and T is Kelvin temperature [39, 65]. According to the relationship between I_{pc} and v mentioned above, it can come to the conclusion that Γ is 6.45×10^{-9} mol cm^{-2}. This value is relatively large, indicating that there are multiple active sites on the modified electrode surface. The high surface active coverage is because of the high ratio superficial area of RGO and the easy functionalization of AuNPs, which enables the electrode surface to be connected with more active substance Fc-ssDNAzyme. The vitality of the electrode is very high, so the modification of the electrode is meaningful.

Optimization of the experimental conditions

Before the experiments were carried out, some experimental conditions were optimized. The added volume of RGO and Fc-ssDNAzyme solution, pH, the culture time, and temperature after adding Pb^{2+} were optimized. Other experiments were implemented at room temperature, which illustrated the applicability of the biosensor.

The volume of RGO will affect the surface coverage of DNA, AuNPs, and the response sensitivity of biosensor. As shown in Fig. S3A (see ESM), the current signal increased with the increase of RGO volume and reached the maximum at 12 μL. While the signal weakened with further increase of RGO volume. Therefore, the optimum volume of RGO was 12 μL. Furthermore, excessive ssDNAzyme is not conducive for the effective immobilization of the probe, which may lead to the increase of non-chemisorption and background signal. As shown in Fig. S3B (see ESM), the effects of different volumes of ssDNAzyme on the current signal were studied. The current value increased with the increase of ssDNAzyme volume, and reached the maximum at 10 μL, so 10 μL was selected as the best volume of ssDNAzyme. The value of pH also played an important role in electrochemical biosensor experiments. Figure S3C (see ESM) manifested the current response values of different pH tested with DPV. After P/AuNPs/RGO-modified electrode reacted with 10,000.0 nM Pb^{2+}, it was tested in PBS solution with different pH. When the pH reached 7.4, the current signal was the largest. The results showed that the most suitable buffer pH was 7.4. In addition, the effects of reaction time and temperature of the modified electrode with Pb^{2+} on the biosensor were also studied since these two parameters could affect the

cleavage effect of Pb^{2+} on hairpin structure. Figure S3D and Fig. S3E (see ESM) exhibited the signal responses of modified electrodes at different culture times and temperatures with 10,000.0 nM Pb^{2+}. It can be seen from the figure that the optimum reaction time and temperature appeared at 40 min and 37 °C, respectively. Thus, after the electrode was immersed in 200 μL Pb^{2+}, it needed to maintain 40 min in 37 °C water bath.

Sensitivity test

Different amounts of Pb^{2+} standard solution were added to the ultra-pure water, various concentrations of Pb^{2+} solutions (0, 0.05, 0.1, 0.5, 1.0, 5.0, 10.0, 50.0, 100.0, 500.0, 1000.0, 5000.0, 10,000.0, 50,000.0, 100,000.0, 400,000.0 nM) were obtained. Under the optimum experimental conditions, the biosensor was used to test the Pb^{2+} concentration by DPV electrochemical method. In the absence of Pb^{2+}, Fc signal molecules existed on the electrode surface because the hairpin structures were not degraded, resulting in a corresponding response signal (background signal). However, in the existence of Pb^{2+}, the hybrid hairpin structure was broken, then Fc was far away from the electrode surface. The charge transfer resistance for $[Fe(CN)_6]^{3-/4-}$ was reduced, so the electrical signal increased. And the electrical signal augmented with the augment of Pb^{2+} concentration (Fig. 4A). The results exhibited that the logarithm of Pb^{2+} concentrations and the current peak values are linearly related in the range of 0.05–400,000.0 nM of Pb^{2+}solution. Moreover, the detection limit was calculated to be 0.015 nM (the average value of the background signal value without Pb^{2+} plus three times the standard deviation (3σ) of the blank background current value) (Fig. 4B). Each point was the result of three independent experiments. The correlation coefficient of the linear equation was 0.99904. Moreover, the relative standard deviation (RSD) was less than 2.77%. Table S2 (see ESM) summarized some previous reports about Pb^{2+} detection sensors. In this work, the biosensor used ferrocene as a signal molecule and additionally added ferricyanide as a redox probe to make detection more sensitive. The use of single-stranded DNAzyme simplified the operation steps. The combination of the advantages of RGO and AuNPs had improved the overall sensitivity of the biosensor. Chemical bond connection between electrode material and DNAzyme made the detection results more reliable. Therefore, the biosensor has a wide detection range and a low detection limit for Pb^{2+}.

Selectivity for Pb^{2+}

To demonstrate the selectivity of the proposed biosensor to Pb^{2+}, the succeeding experiments were underway.

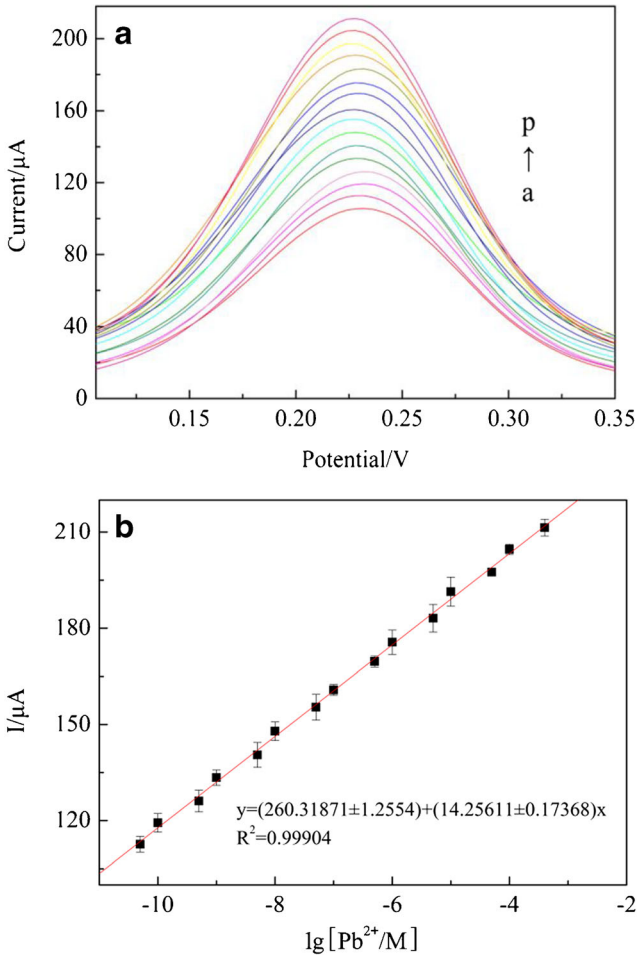

Fig. 4 (**a**) DPV curves of the biosensor at different concentrations of Pb^{2+} (from a to p: 0, 0.05, 0.1, 0.5, 1.0, 5.0, 10.0, 50.0, 100.0, 500.0, 1000.0, 5000.0, 10,000.0, 50,000.0, 100,000.0, and 400,000.0 nM). (**b**) The linear relationship among the peak currents of DPV and logarithm of Pb^{2+} concentrations. Error bars represent the standard deviation for the average of three repeated independent tests

Firstly, the biosensor was used to measure the DPV of Ag^{+}, Al^{3+}, Ca^{2+}, Cd^{2+}, Co^{2+}, Cu^{2+}, Fe^{3+}, Hg^{2+}, K^{+}, Mg^{2+}, Mn^{2+}, Ni^{2+}, and Zn^{2+} of 100,000.0 nM under the optimized conditions. As displayed in Fig. 5, the detection signals of these ions were low ($\triangle I$ represents the measured current value of the metal ion minus the blank background signal value that does not contain any metal ion. The concentration of Pb^{2+} was 1000.0 nM, and the concentration of other metal ions was 100,000.0 nM. Secondly, these ions were mixed with Pb^{2+} (the concentration of Pb^{2+} was 1000.0 nM, and the concentration of other metal ions was 100,000.0 nM), and the current signal measured by the biosensor was relatively high. The results revealed that the biosensor had specific selectivity and sensitivity to Pb^{2+} detection and can resist the interference of other high concentration metal ions.

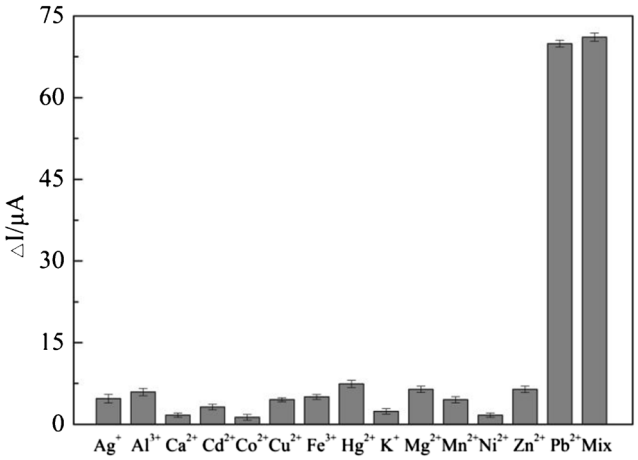

Fig. 5 Selectivity of the Pb^{2+} biosensor. Concentration of Pb^{2+} is 1000.0 nM and of the other metal ions is 100,000.0 nM. The error bars are derived from the standard deviation calculated by three independent experiments. Mix is a mixture of all metal ions, including Pb^{2+}

Practical application of the Pb^{2+} biosensor

To verify the practicability of the biosensor, the water samples in three environments with 0, 100.0, 10,000.0, and 100,000.0 nM Pb^{2+} solution were tested, respectively. Water samples included river water, lake water, and tap water. The sample was first filtered by 0.22 μm membrane, then the Pb^{2+} standard solution was added, and finally, the sample was detected. The results of Pb^{2+} concentration measured by the proposed method and ICP-MS are compared. As shown in Table 1, the results were in good agreement with those measured by ICP-MS, with the maximum RSD of 3.28%. The results certified that the biosensor has a good accuracy in the detection of environmental water samples.

Reproducibility and stability of the RGO-AuNPs-based biosensor

The reproducibility of the modified electrode was detected under the optimal experimental conditions, and 1000.0 nM Pb^{2+} was tested with five different electrodes in the same batch. The results proved that the measured values of the modified electrode were similar, and the maximum RSD was 1.48% (ESM Fig. S4A). The results illustrated that the biosensor had good reproducibility. In order to further prove the reproducibility, the currents of 5.0 nM, 500.0 nM, and 50,000.0 nM Pb^{2+} were determined with the same electrode under the optimum conditions, and the results showed that RSD ≤ 1.18%. Consequently, Fig. S4B (see ESM) further proved that the biosensor had good reproducibility. The modified electrode was stored in the refrigerator (4 °C) for 28 days, and then the current value on the electrode surface was measured at different times (ESM Fig. S4C). With time, the signal value decreased gradually (RSD ≤ 0.68%). In the first week, the current signal decreased at the fastest rate of 9.0%, and then gradually slowed down. After 28 days, the current signal decreased by 12.5%. However, the decrease was normal, because DNAzyme was stored for a long time, it may be deactivated, and in the process of each electrochemical testing, the electrodes were directly immersed in the electrolyte, and part of the AuNPs/RGO particles would inevitably fall off the surface of the electrode. Overall, it was demonstrated that the biosensor had good stability.

Conclusions

The biosensor was designed by using RGO-AuNPs-modified GCE and simple Fc-ssDNAzyme for the specific detection of

Table 1 Detection of Pb^{2+} in environmental samples by the proposed biosensor

Samples	Added (nM)	Found[a] (nM)	Recovery (%)	RSD[b] (%)	ICP-MS[a] (nM)
River water	0	[c]	–	0	< 0.1
	100.0	100.51	100.51	1.71	101.36
	10,000.0	10,113.22	101.13	2.91	10,203.75
	100,000.0	99,927.11	99.93	2.79	99,731.19
Lake water	0	[c]	–	0	< 0.1
	100.0	100.09	100.09	2.67	102.22
	10,000.0	9894.31	98.94	1.75	9754.81
	100,000.0	100,348.56	100.35	3.28	100,517.23
Tap water	0	[c]	–	0	< 0.1
	100.0	99.78	99.78	1.55	98.63
	10,000.0	9691.79	96.92	2.13	9741.92
	100,000.0	100,916.37	100.92	2.45	101,258.51

[a] The average value of the measured values of the three independent experiments

[b] *RSD* relative signal deviation

[c] No Pb^{2+} was found

Pb^{2+}. The detection signal was amplified, which made the detection range of Pb^{2+} wider and the detection limit lower. Consequently, the biosensor had good sensitivity. Moreover, the biosensor had good selectivity, reproducibility, and stability. As a result, the biosensor provided a good electrochemical detection approach for determining the concentration of Pb^{2+} in environmental water samples. Besides, the biosensor can be extended since various enzymes with specificity can be used to detect other different metal ions or organic compounds, etc.

Funding information This work was supported by the Program of National Natural Science Foundation of China (51779090, 51408206, 41601272, 51579098, 51709101, 51521006, 51809090), Hunan Provincial Science and Technology Plan Project (2017SK2243, 2018SK20410, 2016RS3026), the National Program for Support of Top-Notch Young Professionals of China (2014), the Program for Changjiang Scholars and Innovative Research Team in University (IRT-13R17), and the Fundamental Research Funds for the Central Universities (531119200086, 531118010114, 531118040083).

Compliance with ethical standards

Conflict of interest The authors declare that they have no competing interests.

References

1. Chen P, Greenberg B, Taghavi S, Romano C, van der Lelie D, He C. An exceptionally selective lead(II)-regulatory protein from Ralstonia metallidurans: development of a fluorescent lead(II) probe. Angew Chem. 2005;117(18):2775–9.
2. Wang M, Zhang S, Ye Z, Peng D, He L, Yan F, et al. A gold electrode modified with amino-modified reduced graphene oxide, ion specific DNA and DNAzyme for dual electrochemical determination of Pb(II) and Hg(II). Microchim Acta. 2015;182(13–14): 2251–8.
3. Li F, Yang L, Chen M, Li P, Tang B. A selective amperometric sensing platform for lead based on target-induced strand release. Analyst. 2013;138(2):461–6.
4. Li B, Lai C, Zeng G, Qin L, Yi H, Huang D, et al. Facile hydrothermal synthesis of Z-scheme $Bi_2Fe_4O_9/Bi_2WO_6$ heterojunction photocatalyst with enhanced visible light photocatalytic activity. ACS Appl Mater Interfaces. 2018;10(22):18824–36.
5. Yang X, Xu J, Tang X, Liu H, Tian D. A novel electrochemical DNAzyme sensor for the amplified detection of Pb^{2+} ions. Chem Commun. 2010;46(18):3107–9.
6. Zhang C, Zeng G, Huang D, Lai C, Huang C, Li N, et al. Combined removal of di(2-ethylhexyl)phthalate (DEHP) and Pb(II) by using a cutinase loaded nanoporous gold-polyethyleneimine adsorbent. RSC Adv. 2014;4(98):55511–8.
7. Chen B, Wang Z, Hu D, Ma Q, Huang L, Xv C, et al. Scanometric nanomolar lead(II) detection using DNA-functionalized gold nanoparticles and silver stain enhancement. Sensors Actuators B Chem. 2014;200:310–6.
8. Li L, Lai C, Huang F, Cheng M, Zeng G, Huang D, et al. Degradation of naphthalene with magnetic bio-char activate hydrogen peroxide: synergism of bio-char and Fe–Mn binary oxides. Water Res. 2019;160:238–48.
9. Bansod B, Kumar T, Thakur R, Rana S, Singh I. A review on various electrochemical techniques for heavy metal ions detection with different sensing platforms. Biosens Bioelectron. 2017;94: 443–55.
10. Zhang M, Lai C, Li B, Huang D, Zeng G, Xu P, et al. Rational design 2D/2D BiOBr/CDs/g-C_3N_4 Z-scheme heterojunction photocatalyst with carbon dots as solid-state electron mediators for enhanced visible and NIR photocatalytic activity: kinetics, intermediates, and mechanism insight. J Catal. 2019;369:469–81.
11. Yun W, Cai D, Jiang J, Zhao P, Huang Y, Sang G. Enzyme-free and label-free ultra-sensitive colorimetric detection of Pb^{2+} using molecular beacon and DNAzyme based amplification strategy. Biosens Bioelectron. 2016;80:187–93.
12. Gui S, Huang Y, Zhu Y, Jin Y, Zhao R. Biomimetic sensing system for tracing Pb^{2+} distribution in living cells based on the metal-peptide supramolecular assembly. ACS Appl Mater Interfaces. 2019;11(6):5804–11.
13. Niu X, Zhong Y, Chen R, Wang F, Liu Y, Luo D. A "turn-on" fluorescence sensor for Pb^{2+} detection based on graphene quantum dots and gold nanoparticles. Sensors Actuators B Chem. 2018;255: 1577–81.
14. Cai W, Xie S, Zhang J, Tang D, Tang Y. Immobilized-free miniaturized electrochemical sensing system for Pb^{2+} detection based on dual Pb^{2+}-DNAzyme assistant feedback amplification strategy. Biosens Bioelectron. 2018;117:312–8.
15. Yu Y, Yu C, Niu Y, Chen J, Zhao Y, Zhang Y, et al. Target triggered cleavage effect of DNAzyme: relying on Pd-Pt alloys functionalized Fe-MOFs for amplified detection of Pb^{2+}. Biosens Bioelectron. 2018;101:297–303.
16. Zhou Y, Tang L, Zeng G, Zhang C, Xie X, Liu Y, et al. Label free detection of lead using impedimetric sensor based on ordered mesoporous carbon-gold nanoparticles and DNAzyme catalytic beacons. Talanta. 2016;146:641–7.
17. Shi JJ, Zhu JC, Zhao M, Wang Y, Yang P, He J. Ultrasensitive photoelectrochemical aptasensor for lead ion detection based on sensitization effect of CdTe QDs on MoS_2-CdS:Mn nanocomposites by the formation of G-quadruplex structure. Talanta. 2018;183: 237–44.
18. Peng B, Tang L, Zeng G, Fang S, Ouyang X, Long B, et al. Self-powered photoelectrochemical aptasensor based on phosphorus doped porous ultrathin g-C_3N_4 nanosheets enhanced by surface plasmon resonance effect. Biosens Bioelectron. 2018;121:19–26.
19. Liao X, Luo J, Wu J, Fan T, Yao Y, Gao F, et al. A sensitive DNAzyme-based electrochemical sensor for Pb^{2+} detection with platinum nanoparticles decorated TiO_2/α-Fe_2O_3 nanocomposite as signal labels. J Electroanal Chem. 2018;829:129–37.
20. Taghdisi SM, Danesh NM, Lavaee P, Ramezani M, Abnous K. An electrochemical aptasensor based on gold nanoparticles, thionine and hairpin structure of complementary strand of aptamer for ultrasensitive detection of lead. Sensors Actuators B Chem. 2016;234: 462–9.
21. Zhang Y, Xiao S, Li H, Liu H, Pang P, Wang H, et al. A Pb^{2+}-ion electrochemical biosensor based on single-stranded DNAzyme catalytic beacon. Sensors Actuators B Chem. 2016;222:1083–9.
22. Chen X, Tian R, Zhang Q, Yao C. Target-induced electronic switch for ultrasensitive detection of Pb^{2+} based on three dimensionally ordered macroporous Au-Pd bimetallic electrode. Biosens Bioelectron. 2014;53:90–8.
23. Huang D, Liu X, Lai C, Qin L, Zhang C, Yi H, et al. Colorimetric determination of mercury(II) using gold nanoparticles and double ligand exchange. Microchim Acta. 2018;186(31):1–8.
24. Yi X, Rowe AA, Plaxco KW. Electrochemical detection of parts-per-billion lead via an electrode-bound DNAzyme assembly. J Am Chem Soc. 2007;129(2):262–3.
25. Wang Z, Lee JH, Lu Y. Label-free colorimetric detection of lead ions with a nanomolar detection limit and tunable dynamic range by using gold nanoparticles and DNAzyme. Adv Mater. 2008;20(17): 3263–7.

26. Zhang C, Lai C, Zeng G, Huang D, Tang L, Yang C, et al. Nanoporous Au-based chronocoulometric aptasensor for amplified detection of Pb^{2+} using DNAzyme modified with Au nanoparticles. Biosens Bioelectron. 2016;81:61–7.
27. Farzin L, Shamsipur M, Sheibani S. A review: aptamer-based analytical strategies using the nanomaterials for environmental and human monitoring of toxic heavy metals. Talanta. 2017;174:619–27.
28. Khalil I, Rahmati S, Muhd Julkapli N, Yehye WA. Graphene metal nanocomposites—recent progress in electrochemical biosensing applications. J Ind Eng Chem. 2018;59:425–39.
29. Liu X, Huang D, Lai C, Qin L, Zeng G, Xu P, et al. Peroxidase-like activity of smart nanomaterials and their advanced application in colorimetric glucose biosensors. Small. 2019:1–27.
30. Wang Z, Yu J, Gui R, Jin H, Xia Y. Carbon nanomaterials-based electrochemical aptasensors. Biosens Bioelectron. 2016;79:136–49.
31. Liu X, Huang D, Lai C, Zeng G, Qin L, Zhang C, et al. Recent advances in sensors for tetracycline antibiotics and their applications. TrAC Trends Anal Chem. 2018;109:260–74.
32. Molina J, Cases F, Moretto LM. Graphene-based materials for the electrochemical determination of hazardous ions. Anal Chim Acta. 2016;946:9–39.
33. Ioniță M, Vlăsceanu GM, Watzlawek AA, Voicu SI, Burns JS, Iovu H. Graphene and functionalized graphene: extraordinary prospects for nanobiocomposite materials. Composites Part B. 2017;121:34–57.
34. Li B, Lai C, Zeng G, Huang D, Qin L, Zhang M, et al. Black phosphorus, a rising star 2D nanomaterial in the post-graphene era: synthesis, properties, modifications, and photocatalysis applications. Small. 2019;15(8):1–30.
35. Novoselov KS, Geim AK, Morozov SV, Jiang D, ., Zhang Y, ., Dubonos SV et al. Electric field effect in atomically thin carbon films. Science. 2004;306(5696):666–669.
36. Yi H, Yan M, Huang D, Zeng G, Lai C, Li M, et al. Synergistic effect of artificial enzyme and 2D nano-structured Bi_2WO_6 for eco-friendly and efficient biomimetic photocatalysis. Appl Catal B. 2019;250:52–62.
37. Kochmann S, Hirsch T, Wolfbeis OS. Graphenes in chemical sensors and biosensors. TrAC Trends Anal Chem. 2012;39:87–113.
38. Lawal AT. Progress in utilisation of graphene for electrochemical biosensors. Biosens Bioelectron. 2018;106:149–78.
39. Gao F, Gao C, He S, Wang Q, Wu A. Label-free electrochemical lead(II) aptasensor using thionine as the signaling molecule and graphene as signal-enhancing platform. Biosens Bioelectron. 2016;81:15–22.
40. Zhang Y, Xie J, Liu Y, Pang P, Feng L, Wang H, et al. Simple and signal-off electrochemical biosensor for mercury(II) based on thymine-mercury-thymine hybridization directly on graphene. Electrochim Acta. 2015;170:210–7.
41. He S, Song B, Li D, Zhu C, Qi W, Wen Y, et al. A graphene nanoprobe for rapid, sensitive, and multicolor fluorescent DNA analysis. Adv Funct Mater. 2010;20(3):453–9.
42. Rasheed PA, Sandhyarani N. Graphene-DNA electrochemical sensor for the sensitive detection of BRCA1 gene. Sensors Actuators B Chem. 2014;204:777–82.
43. Benvidi A, Rajabzadeh N, Mazloum-Ardakani M, Heidari MM, Mulchandani A. Simple and label-free electrochemical impedance Amelogenin gene hybridization biosensing based on reduced graphene oxide. Biosens Bioelectron. 2014;58:145–52.
44. Lu Z, Yang S, Yang Q, Luo S, Liu C, Tang Y. A glassy carbon electrode modified with graphene, gold nanoparticles and chitosan for ultrasensitive determination of lead(II). Microchim Acta. 2013;180(7–8):555–62.
45. Qin L, Yi H, Zeng G, Lai C, Huang D, Xu P, et al. Hierarchical porous carbon material restricted Au catalyst for highly catalytic reduction of nitroaromatics. J Hazard Mater. 2019;380:1–11.
46. Lai C, Liu X, Qin L, Zhang C, Zeng G, Huang D, et al. Chitosan-wrapped gold nanoparticles for hydrogen-bonding recognition and colorimetric determination of the antibiotic kanamycin. Microchim Acta. 2017;184(7):2097–105.
47. Zhou X, Lai C, Huang D, Zeng G, Chen L, Qin L, et al. Preparation of water-compatible molecularly imprinted thiol-functionalized activated titanium dioxide: selective adsorption and efficient photodegradation of 2, 4-dinitrophenol in aqueous solution. J Hazard Mater. 2018;346:113–23.
48. Qin L, Zeng G, Lai C, Huang D, Zhang C, Xu P, et al. A visual application of gold nanoparticles: simple, reliable and sensitive detection of kanamycin based on hydrogen-bonding recognition. Sensors Actuators B Chem. 2017;243:946–54.
49. Fu Y, Qin L, Huang D, Zeng G, Lai C, Li B, et al. Chitosan functionalized activated coke for Au nanoparticles anchoring: green synthesis and catalytic activities in hydrogenation of nitrophenols and azo dyes. Appl Catal B. 2019;255:1–11.
50. Saleem W, Salinas C, Watkins B, Garvey G, Sharma AC, Ghosh R. Antibody functionalized graphene biosensor for label-free electrochemical immunosensing of fibrinogen, an indicator of trauma induced coagulopathy. Biosens Bioelectron. 2016;86:522–9.
51. Hamsawahini K, Sathishkumar P, Ahamad R, Yusoff AR. A sensitive, selective and rapid determination of lead(II) ions in real-life samples using an electrochemically reduced graphene oxide-graphite reinforced carbon electrode. Talanta. 2015;144:969–76.
52. Jr WSH, Offeman RE. Preparation of graphitic oxide. J Am Chem Soc. 1958;80(6):1339.
53. Pang P, Liu Y, Zhang Y, Gao Y, Hu Q. Electrochemical determination of luteolin in peanut hulls using graphene and hydroxyapatite nanocomposite modified electrode. Sensors Actuators B Chem. 2014;194:397–403.
54. Zhang Y, Xiao S, Xie J, Yang Z, Pang P, Gao Y. Simultaneous electrochemical determination of catechol and hydroquinone based on graphene–TiO_2 nanocomposite modified glassy carbon electrode. Sensors Actuators B Chem. 2014;204:102–8.
55. Zhu X, Sun L, Chen Y, Ye Z, Shen Z, Li G. Combination of cascade chemical reactions with graphene-DNA interaction to develop new strategy for biosensor fabrication. Biosens Bioelectron. 2013;47:32–7.
56. Lee PM, Wang Z, Liu X, Chen Z, Liu E. Glassy carbon electrode modified by graphene–gold nanocomposite coating for detection of trace lead ions in acetate buffer solution. Thin Solid Films. 2015;584:85–9.
57. Peng Y, Li L, Yi X, Guo L. Label-free picomolar detection of Pb^{2+} using atypical icosahedra gold nanoparticles and rolling circle amplification. Biosens Bioelectron. 2014;59:314–20.
58. Zhang B, Chen J, Liu B, Tang D. Amplified electrochemical sensing of lead ion based on DNA-mediated self-assembly-catalyzed polymerization. Biosens Bioelectron. 2015;69:230–4.
59. Lai C, Liu S, Zhang C, Zeng G, Huang D, Qin L, et al. Electrochemical aptasensor based on sulfur-nitrogen codoped ordered mesoporous carbon and thymine-Hg^{2+}-thymine mismatch structure for Hg^{2+} detection. ACS Sens. 2018;3(12):2566–73.
60. Levicky R, Herne TM, Tarlov MJ, Satija SK. Using self-assembly to control the structure of DNA monolayers on gold: a neutron reflectivity study. J Am Chem Soc. 1998;120(38):9787–92.
61. Tang S, Tong P, You X, Lu W, Chen J, Li G, et al. Label free electrochemical sensor for Pb^{2+} based on graphene oxide mediated deposition of silver nanoparticles. Electrochim Acta. 2016;187:286–92.
62. Tang L, Wang Y, Li J. The graphene/nucleic acid nanobiointerface. Chem Soc Rev. 2015;44(19):6954–80.

63. Zeng G, Zhang C, Huang D, Lai C, Tang L, Zhou Y, et al. Practical and regenerable electrochemical aptasensor based on nanoporous gold and thymine-Hg^{2+}-thymine base pairs for Hg^{2+} detection. Biosens Bioelectron. 2017;90:542–8.
64. Wen Y, Peng C, Li D, Zhuo L, He S, Wang L, et al. Metal ion-modulated graphene-DNAzyme interactions: design of a nanoprobe for fluorescent detection of lead(II) ions with high sensitivity, selectivity and tunable dynamic range. Chem Commun. 2011;47(22): 6278–80.
65. Xiao Q, Feng J, Li J, Feng M, Huang S. A label-free and ultrasensitive electrochemical aptasensor for lead(II) using a N,P dual-doped carbon dot-chitosan composite as a signal-enhancing platform and thionine as a signaling molecule. Analyst. 2018;143(19): 4764–73.